THE JOURNAL OF PHYSICAL CHEMISTRY A

pubs.acs.org/JPCA

Article

Aromaticity of Even-Number Cyclo[*n*]carbons (*n* = 6−100)

Glib V. Baryshnikov,* Rashid R. Valiev,* Rinat T. Nasibullin, Dage Sundholm, Theo Kurten, and Hans Ågren

Cite This: *J. Phys. Chem. A* 2020, 124, 10849−10855

Read Online

ACCESS | Metrics & More | Article Recommendations | Supporting Information

ABSTRACT: The recently synthesized cyclo[18]carbon molecule has been characterized in a number of studies by calculating electronic, spectroscopic, and mechanical properties. However, cyclo[18]carbon is only one member of the class of cyclo[*n*]carbons—standalone carbon allotrope representatives. Many of the larger members of this class of molecules have not been thoroughly investigated. In this work, we calculate the magnetically induced current density of cyclo[*n*]carbons in order to elucidate how electron delocalization and aromatic properties change with the size of the molecular ring (*n*), where *n* is an even number between 6 and 100. We find that the Hückel rules for aromaticity (4*k* + 2) and antiaromaticity (4*k*) become degenerate for large C_n rings (*n* > 50), which can be understood as a transition from a delocalized electronic structure to a nonaromatic structure with localized current density fluxes in the triple bonds. Actually, the calculations suggest that cyclo[*n*]carbons with *n* > 50 are nonaromatic cyclic polyalkynes. The influence of the amount of nonlocal exchange and the asymptotic behavior of the exchange−correlation potential of the employed density functionals on the strength of the magnetically induced ring current and the aromatic character of the large cyclo[*n*]carbons is also discussed.

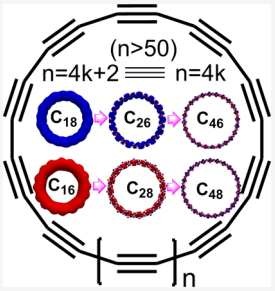

INTRODUCTION

Since the recent synthesis of cyclo[18]carbon,[1] a large number of studies of spectroscopic,[2−4] aromatic,[5−10] structural,[5,10−14] mechanical,[15] and electronic properties[7,16−21] of cyclo[*n*]-carbons have been reported. Recently, Anderson *et al.*[22] proposed a more efficient protocol for synthesizing cyclo[18]-carbon. Thus, one can expect that also other cyclo[*n*]carbons will be synthesized in the near future. Cyclo[*n*]carbons absorb light in the near-UV region and have a number of low-lying excited states that can be reached by dipole-forbidden electronic transitions from the ground state, implying that the de-excitation from them is not expected to lead to any luminescence.[2] Cyclo[*n*]carbons should on the other hand exhibit extraordinary reactivity because of the −C≡C triple bonds, implying that they may be used as precursors for graphene allotropes.[23] It has also been suggested that cyclo[18]carbon can function as an electron acceptor[24] and form metal complexes[21] and catenanes.[6] The reactivity of cyclo[*n*]carbons also depends on their degree of aromaticity, that is, to the extent of the delocalization of the π electrons around the ring. The aromaticity of cyclo[*n*]carbons has been studied in a number of works focusing on the double antiaromaticity/aromaticity of molecules with (4*k*) and (4*k* + 2) (*k* = 1−7) π electrons.[5−10,25−27] The studies show that for small *n* values, the (4*k* + 2) cyclo[*n*]carbons are indeed doubly aromatic with two subsystems of the delocalized (4*k* + 2) π electrons. The cyclo[*n*]carbons were found to have delocalized π electrons in the molecular plane inside and outside the ring, which is denoted as "in" in Scheme 1. There is an independent delocalized π-electron system out of the molecular plane above and below the ring, denoted as "out" in Scheme 1. For cyclo[18]carbon, the two delocalized donut-like π-electron systems contain 18π electrons each.[5,7,10,25] The two π-electron systems are not identical because the p_{in} orbitals on the outside of the ring have a slightly smaller overlap than the p_{out} orbitals because of the bent curvature of the ring.

Scheme 1. Electronic Structure of Cyclo[*n*]carbons (Left) and Formal Chemical Structure of Cyclo[18]carbon (Right)

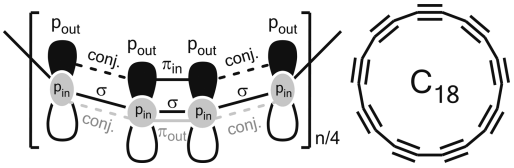

Fowler *et al.* studied the double aromaticity of cyclo[*n*]-carbons with *n* = 6−30 and the interplay between the π_{in} and π_{out} electron systems.[25] They found that the aromatic properties of the two delocalized subsystems are independent, obeying the Hückel rule of aromaticity.[25] The aromatic properties of cyclo[*n*]carbons have also been studied by calculating nucleus-independent chemical shift (NICS) values in the center of the molecular ring.[9,25,28] Such NICS values are, however, not a very reliable aromaticity criterion because the

Received: October 27, 2020
Revised: November 26, 2020
Published: December 10, 2020

https://dx.doi.org/10.1021/acs.jpca.0c09692
J. Phys. Chem. A 2020, 124, 10849−10855

radius of the ring increases with the increasing number of carbon atoms in the ring, making the ring center further distant from the delocalized electrons in the larger cyclo[n]carbons. The NICS values in the center of the ring therefore decrease when expanding the ring, even though the ring would sustain a ring current of the same strength as for a smaller ring.

Seenithurai and Chai[29] recently reported a systematic density functional theory (DFT) study of the energy differences between the lowest singlet and triplet states and between the lowest singlet and quintet states of cyclo[n]-carbons (n = 8−100). They also reported ionization potentials, electron affinities, fundamental gaps, occupation numbers of the frontier orbitals, and the relative energy with respect to the linear isomers. Their calculations yielded similar trends as obtained in earlier studies.[8,25,28] For small cyclo[n]carbons with n < 32, there is a clear difference between the properties of the rings with ($4k$ + 2) and ($4k$) carbon atoms, whereas for larger cyclo[n]carbons, the molecules with ($4k$ + 2) and ($4k$) carbon atoms have similar properties. Even though they studied electronic properties that are related to aromaticity and electron delocalization, they did not explicitly discuss the Hückel aromaticity and antiaromaticity of the cyclo[n]carbons.

We recently reported calculations of aromatic properties of Hückel antiaromatic ($4k$) cyclo[n]carbons.[30] The calculations of magnetically induced current densities showed that the ring current strength decreases with increasing n. For cyclo[44]-carbon, the aromatic character switches from antiaromatic to aromatic, that is, the net ring current is paratropic for cyclo[40]carbon, while the ring current is unexpectedly diatropic for cyclo[44]carbon. The underlying reason for the switch from the antiaromatic to aromatic character was not elucidated.

In this work, we perform systematic studies of the electronic structure and the aromatic character of cyclo[n]carbons with n = 6−100. The calculations show that the Hückel antiaromatic ($4k$) and Hückel aromatic ($4k$ + 2) cyclo[n]carbons become nonaromatic for n > 50. Thus, large cyclo[n]carbons can be considered as unsaturated carbon rings with localized single and triple bonds, which may be useful information for future synthesis of large cyclo[n]carbons.

COMPUTATIONAL DETAILS

The molecular structures of the cyclo[n]carbons (n = 6−100) were initially optimized at the DFT level using the M06-2X functional and the def2-TZVP basis set.[31,32] It has previously been shown[5,10] that only density functionals with a large amount of nonlocal Hartree−Fock exchange (>40%) yield the correct alternation of single and triple bonds in ($4k$ + 2) cyclo[n]carbons starting from the C_{14} molecule, while the use of density functionals with no or a moderate amount of Hartree−Fock exchange results in the incorrect cumulenic structure for C_{14} and C_{18}. Optimizations at the BHLYP/def2-TZVP[32−34] and ωB97XD/def2-TZVP[32,35] levels have been performed in order to investigate the unexpected oscillations in the strength of the magnetically induced ring current for cyclo[n]carbons in the range of n = 36−52 that were obtained at the M06-2X/def2-TZVP level. Calculations at the M06-L/def2-TZVP[32,36] level (0% Hartree−Fock exchange) have also been carried out for the C_{36}−C_{52} series in order to assess the role of Hartree−Fock exchange.

The applicability of the employed DFT methods for studies of large cyclo[n]carbons was checked by calculating the electronic structure of the singlet ground state of cyclo[n]-carbons (n = 30, 40, 50, 60, 70, 80, 90, and 100) at the complete active space self-consistent field (CASSCF) level.[37,38] For the ($4k$ + 2) systems (C_{30}, C_{50}, C_{70}, and C_{90}), the (8, 8) active space was used (eight active electrons in eight active orbitals) and for the ($4k$) molecules (C_{40}, C_{60}, C_{80}, and C_{100}), the (12, 12) CASSCF scheme was employed. In the single-point CASSCF calculations, we used the 6-31G(d,p),[39−41] 6-311G(d,p),[40−42] and cc-pVTZ[43] basis sets and the BHLYP/def2-TZVP-optimized molecular structures because this level of theory gives the expected and most likely correct dependence of the strength of the magnetically induced ring current on the size of the ring.

The calculations showed that the studied molecules have a closed-shell singlet ground state dominated by a single-reference configuration. The CASSCF calculations were performed with the Firefly software.[44,45] The GIMIC code[46−48] was used for calculating the magnetically induced current densities and for integrating the ring current strengths. Gauge-independent magnetically induced current densities were calculated using density matrices obtained in the GIAO[49] nuclear magnetic resonance (NMR) shielding calculations. The magnetic field was oriented along the z axis, perpendicular to the plane of the molecular ring. The strengths of the current densities were obtained by numerical integration of the current density passing a rectangular surface perpendicular to the molecule plane. The DFT calculations were performed with the Gaussian 16 software.[50]

RESULTS AND DISCUSSION

Structure of Cyclo[*n*]carbons. The experimental polyalkyne structure of cyclo[18]carbon[1,22] was obtained from the calculations at the DFT level when using functionals with a large amount of Hartree−Fock exchange.[5,12] In this work, we have optimized the molecular structures using the M06-2X, BHLYP, and ωB97XD functionals, which yielded a polyalkyne structure for cyclo[18]carbon. The Cartesian coordinates of the molecular structures can be found in the Supporting Information. Cyclo[14]carbon is an intermediate between the cumulene structures of C_6 and C_{10} and the polyalkyne-like structure of C_{18}. The larger cyclo[n]carbons consisting of ($4k$ + 2) carbon atoms have even more pronounced polyalkyne structures. The Peierls transition of the molecular structure has been reported to occur for cyclo[n]carbons with n = 14, 18, or 22 depending on the employed computational level.[25,51,52] In our calculations using the M06-2X, BHLYP, and ωB97XD functionals, the Peierls transition occurs between C_{14} and C_{18} (Figure 1, Table S1). In addition to the strong bond length alternation (BLA) that appears in C_{18} and the larger cyclo[n]carbons (n = 22−100), the bond angle alternation (BAA) disappears for C_{18} and larger cyclo[n]carbons (Figure 1, Table S2).

For ($4k$) cyclo[n]carbons, the BAA drastically changes from C_{12} (BAA = 30°) to C_{16} (BAA = 0.04°). All larger cyclo[n]carbons (after C_{16}−C_{18}), regardless of whether they are of the ($4k$) or ($4k$ + 2) type, show in principle similar structures with significant BLA but without BAA (Tables S1 and S2). However, the BLA becomes saturated (the BLA difference between two nearest analogues is <0.001 Å) at C_{32}−C_{34}, which approximately matches the size of the cyclo[n]-carbon where the magnetically induced current strength vanishes, showing the importance of BLA as a descriptor of the electron delocalization.

https://dx.doi.org/10.1021/acs.jpca.0c09692
J. Phys. Chem. A 2020, 124, 10849−10855

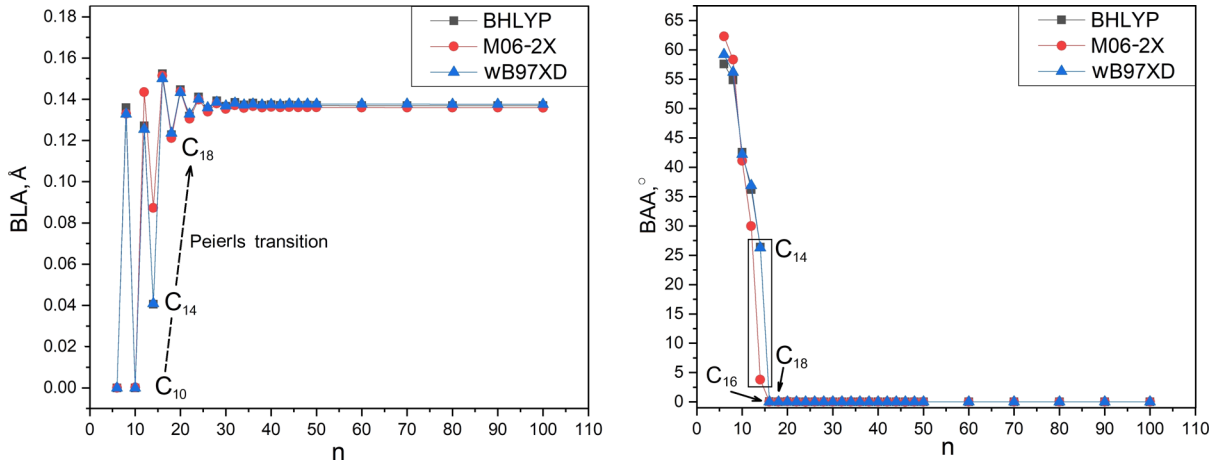

Figure 1. BLA of cyclo[*n*]carbons as a function of *n* is shown in the left graph. The BAA of cyclo[*n*]carbons as a function of *n* is shown in the right graph. BLA and BAA have been calculated for the cyclo[*n*]carbons (*n* = 6−100) using the BHLYP, M06-2X, and ωB97XD functionals.

CASSCF Studies of Cyclo[*n*]carbons. In a recent paper, Seenithurai and Chai[29] employed thermally assisted occupation DFT (TAO-DFT) calculations for investigating the ground electronic state of cyclo[*n*]carbons (*n* = 10−100). Based on the analysis of the occupation numbers of frontier molecular orbitals, they found that the polyradical nature increases with increasing size of the cyclo[*n*]carbon. In order to check this statement, we performed CASSCF calculations for each 10th cyclo[*n*]carbon starting from C_{30}. The results are summarized in Table 1. The results of the CASSCF calculations are basis set independent and give occupation numbers of the active orbitals (*x*) that are close to 2.00 and 0.00, implying that the weight (*w*) of the closed-shell singlet determinant is also close to 1. Thus, we can conclude that all the studied cyclo[*n*]carbons possess a single-reference ground singlet electronic state in sheer contrast to the results obtained in TAO-DFT calculations.

Table 1. Occupation Number (*x*) of the Highest Molecular Orbital with an Occupation Number Near 2 Obtained in the CASSCF Calculation and the Weight (*w*) of Closed-Shell Determinant for the S_0 State Using Different Basis Sets

molecule	6-31G(d,p)	6-311G(d,p)	cc-pvTZ
C_{30}	*x* = 1.94; *w* = 0.95	*x* = 1.95; *w* = 0.94	*x* = 1.94; *w* = 0.94
C_{40}	*x* = 1.94; *w* = 0.94	*x* = 1.94; *w* = 0.91	*x* = 1.94; *w* = 0.91
C_{50}	*x* = 1.94; *w* = 0.94	*x* = 1.92; *w* = 0.94	*x* = 1.99; *w* = 0.99
C_{60}	*x* = 1.94; *w* = 0.91	*x* = 1.92; *w* = 0.94	*x* = 1.99; *w* = 0.99
C_{70}	*x* = 1.98; *w* = 0.96	*x* = 1.92; *w* = 0.94	*x* = 1.99; *w* = 0.99
C_{80}	*x* = 1.94; *w* = 0.92	*x* = 1.92; *w* = 0.91	*x* = 1.99; *w* = 0.99
C_{90}	*x* = 1.99; *w* = 0.99	*x* = 1.92; *w* = 0.90	*x* = 1.99; *w* = 0.99
C_{100}	*x* = 1.99; *w* = 0.99	*x* = 1.91; *w* = 0.90	*x* = 2.00; *w* = 0.99

Aromaticity of Cyclo[*n*]carbons Obtained with GIMIC (*n* = 6−34). Applying the GIMIC approach to the (4*k*) and (4*k* + 2) cyclo[*n*]carbons (*n* = 6−100), one can analyze the distribution of the magnetically induced ring current. The ring current strength is a reliable indicator of the electron delocalization in cyclo[*n*]carbons (*n* = 6−100). Starting from the smallest Hückel aromatic (4*k* + 2) cyclo[*n*]carbon, namely, cyclo[6]carbon with *k* = 1, one can see that it sustains a net diatropic current of 14 nA T^{-1} at the M06-2X, BHLYP, and ωB97XD levels (Table S3), which means that C_6 is aromatic. This agrees with several previous studies[25,26] where C_6 was found to be doubly aromatic because of the delocalization of two sextets of π electrons lying in and out of the molecular plane. Despite that the net current is diatropic for the C_6 ring, a paratropic component can also be seen in the current density map (Figures S1 and S2).

The smallest Hückel antiaromatic (4*k*) cyclo[8]carbon (*k* = 2) considered here is clearly antiaromatic, sustaining a net ring current of −33.3 nA T^{-1} at the BHLYP level of theory. Ring current strengths of −42.3 and −35.7 nA T^{-1} were obtained at the M06-2X and ωB97XD levels, respectively (Table S3). The diatropic contribution to the ring current of C_8 is negligibly small. The strength of the paratropic ring current decreases with *n* for the larger Hückel antiaromatic (4*k*) cyclo[*n*]carbons with *k* = 3−8. The ring current strength of cyclo[32]carbon is −4.6 nA T^{-1} at the BHLYP level. A similar value of −4.3 nA T^{-1} is obtained at the M06-2X level, while the ωB97XD calculations yield a ring current strength of 0.9 nA T^{-1}. The topology of the current density shows that the current density tends to become more localized to the triple bonds with increasing *k* for the (4*k*) cyclo[*n*]carbons (*k* = 3−8). The diatropic contribution to the current density appears at the edge of the triple bonds, which means that the global electron delocalization is broken (Figure S2). The transition from delocalized to localized topology of the current density for the Hückel antiaromatic (4*k*) cyclo[*n*]carbons is clearly seen for C_{28}, whose net paratropic ring current is predominantly delocalized over the ring, whereas the paratropic current density of C_{32} is predominantly localized to the triple bonds (Figure 2). A drastic transition is also seen at C_{28}−C_{32}, whose ring current strengths are −7.9/−4.6, −15.3/−4.3, and −5.4/−0.9 nA T^{-1} at the BHLYP, M06-2X, and ωB97XD levels, respectively (Table S3).

The Hückel aromatic (4*k* + 2) cyclo[*n*]carbons behave similarly but with opposite signs, that is, the direction of the ring current. Judged from the ring current strength, the degree of aromaticity increases from C_6 to C_{14} (Table S3), whereas starting from C_{18}, the net diatropic ring current strength gradually declines with increasing *n* and becomes only 3.9 nA T^{-1} for C_{34} at the BHLYP level. Paratropic contributions appear at each single bond (*i.e.*, between each pair of triple bonds, which are marked with pink dotted lines in Figure 2). The transition from globally delocalized to bond-localized topology of the current density is observed between C_{26} (delocalized) and C_{30} (localized). This transition is accom-

https://dx.doi.org/10.1021/acs.jpca.0c09692
J. Phys. Chem. A 2020, 124, 10849−10855

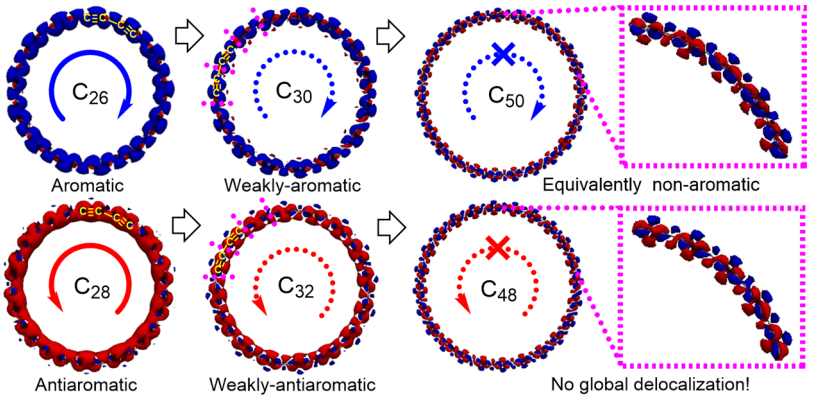

Figure 2. Magnetically induced current density maps for selected $(4k + 2)$ (top) and $(4k)$ (bottom) cyclo[n]carbons (n = 26, 28, 30, 32, 48, and 50) calculated at the BHLYP/def2-TZVP level. The red and blue arrows denote the circulation direction of the paratropic and diatropic magnetically induced ring currents, respectively.

panied by a decrease in the net ring current strength from 10.8 to 6.6 nA T^{-1} at the BHLYP level. Thus, GIMIC calculations predict a gradual decline in the global electron delocalization with increasing n for the cyclo[n]carbons starting from $(4k + 2)$ C_{26} and $(4k)$ C_{28}.

Aromaticity of Cyclo[*n*]carbons from the GIMIC Approach (*n* = 36−100). The $(4k)$ C_{48} and $(4k + 2)$ C_{50} molecules have almost identical current density maps, as seen in Figure 2. Based on the GIMIC calculations, they and the larger cyclo[n]carbons are nonaromatic polyalkynes, which perfectly explains the previously observed saturation of electronic descriptors such as the ionization potential, electron affinity, singlet−triplet splitting, singlet−quintet splitting, and so forth of the larger cyclo[n]carbons.[8,28,29]

GIMIC calculations at the BHLYP level lead to a systematic decline in the ring current strength of the larger cyclo[n]-carbons (n = 36−100). The ring current strengths calculated at the M06-2X level for the cyclo[n]carbons with n = 38−50 differ significantly from the expected trend obtained at the BHLYP level (Figure 3). The ring current strengths calculated in this range using the M06-2X functional are a strongly irregular function of n and not a regularly oscillating function as obtained at the BHLYP level (Figure 3), indicating some

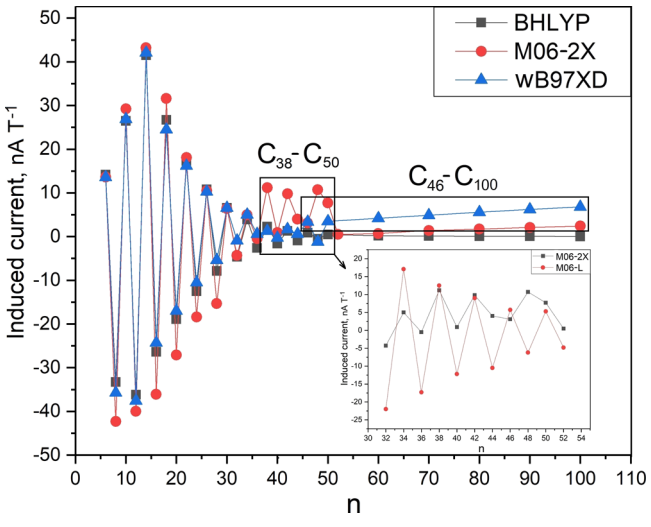

Figure 3. Strength of the magnetically induced current for C_6−C_{44} calculated using different DFT functionals.

limitations of the M06-2X functional for calculating magnetically induced current densities, even though the BHLYP and M06-2X functionals have about the same amount of Hartree−Fock exchange. The two functionals yield similar molecular structures with practically the same BLA and BAA (Tables S1 and S2).

The multireference problem of the ground state of the cyclo[n]carbons could be ruled out based on CASSCF calculations as discussed above. A possible reason for the erroneous oscillations in the C_{38}−C_{50} region obtained at the M06-2X level seems to be an unsuitable parametrization of the functional for calculations of magnetically induced current densities. In the previous GIMIC studies, we successfully used the M06-2X functional in calculations on aromatic and antiaromatic porphyrinoids.[53−55] However, generally, the M06-2X functional exaggerates the diatropic contribution to the ring current,[55,56] which we actually also observe for C_{60}−C_{100}. The strength of the ring current gradually increases from 0.7 nA T^{-1} for C_{44} to 2.4 nA T^{-1} for C_{100} (Figure 3).

The M06-2X functional was also criticized by Stoychev *et al.*, who found that M06-2X was the worst functional for calculating NMR shielding constants among the employed ones.[57] They found that the M06-L functional is much better aimed for such studies.[57] We therefore performed current density calculations using the M06-L functional for the problematic C_{38}−C_{50} molecules (Table S4) and found a similar asymptotic behavior as obtained with the BHLYP functional (the plot is inserted in Figure 3).

We also tested the ωB97XD functional and found a similar trend for C_6−C_{44} as obtained at the BHLYP level. Calculations using the ωB97XD functional suggest that the ring current strength increases with n in the range of C_{44}−C_{100}. The ring current strength gradually increases from 0.6 nA T^{-1} for C_{44} to 6.8 nA T^{-1} for C_{100} (Figure 3). The unexpected increase in the ring current strength obtained with the ωB97XD functional is most likely an artifact, the reason of which has not been elucidated. For large cyclo[n]carbons (n > 44) that sustain localized single and triple bonds, the short-range Hartree−Fock exchange scheme may overestimate exchange interactions[58] that might result in a monotonous increase in magnetically induced ring current strength for increasing size of the cyclo[n]carbons. The BHLYP functional yields reasonable qualitative and quantitative values for the magnetically induced ring current strength for the whole series of the studied C_n (n = 6−100) molecules, whereas the M06-2X and

https://dx.doi.org/10.1021/acs.jpca.0c09692
J. Phys. Chem. A 2020, 124, 10849−10855

ωB97XD functionals yield an unexpected nonasymptotic behavior of the strength of the magnetically induced current density of C_{38}−C_{50} and C_{44}−C_{100}, respectively. However, regardless of the employed DFT functional, the large Hückel antiaromatic ($4k$) and aromatic ($4k + 2$) cyclo[n]carbons have similar molecular structures and strengths of the magnetically induced ring current. Because the large cyclo[n]carbons sustain a very weak ring current, they are nonaromatic according to the ring current criterion.

CONCLUSIONS

A series of cyclo[n]carbons with an even number of carbon atoms in the range of n = 6−100 were studied computationally with the focus on an analysis of the magnetically induced current density, which was used for assessing their aromatic character. All studied cyclo[n]carbons (except C_6, C_{10}, and C_{14}) have a sheer bond length alternation (BLA) corresponding to polyalkyne-type molecules. The saturation limit of the BLA, that is, when the difference in the BLA between two adjacent analogues is <0.001 Å, appears at C_{32}−C_{34}. The bond angle alternation (BAA) vanishes rapidly in the range of n = 6−14 and becomes negligibly small (<0.04°) for C_{16}. Differences in the aromatic character of the ($4k + 2$) cyclo[n]carbons and the antiaromatic character of ($4k$) cyclo[$4n$]carbons are obtained until C_{34} and C_{32}, respectively, which match exactly the saturation limit of the BLA. The BLA can thus be seen as an important structural factor affecting the electron delocalization in cyclo[n]carbons. Based on GIMIC calculations of the ring current strength, we conclude that the complete transformation of the Hückel antiaromatic ($4k$) and Hückel aromatic ($4k + 2$) systems into nonaromatic molecules occurs at n > 50, regardless of whether the molecule has ($4k$) or ($4k + 2$) π electrons in the delocalization pathway around the ring. The GIMIC calculations show that the transformation is due to a transition from a delocalized electronic structure to an electronic structure with localization in the triple bonds. The localized current density in the triple bonds suggests that the larger cyclo[n]carbons are unsaturated nonaromatic cyclic polyalkynes, which might be useful information when developing efficient protocols for synthesizing novel cyclo[n]-carbons, that is, other than C_{18}.

ASSOCIATED CONTENT

Supporting Information

The Supporting Information is available free of charge at https://pubs.acs.org/doi/10.1021/acs.jpca.0c09692.

Structural descriptors BLA and BAA, current density plots and corresponding current strengths, and optimized geometries in Cartesian coordinates of the studied cyclo[n]carbons at different DFT levels (n = 6−100) (PDF)

AUTHOR INFORMATION

Corresponding Authors

Glib V. Baryshnikov − *Department of Physics and Astronomy, Uppsala University, Uppsala SE-751 20, Sweden; Department of Chemistry and Nanomaterials Science, Bohdan Khmelnytsky National University, Cherkasy 18031, Ukraine;* orcid.org/0000-0002-0716-3385; Email: glibar@kth.se

Rashid R. Valiev − *Research School of Chemistry & Applied Biomedical Sciences, National Research Tomsk Polytechnic University, Tomsk 634050, Russia; Department of Chemistry, Faculty of Science, University of Helsinki, Helsinki FIN-00014, Finland;* orcid.org/0000-0002-2088-2608; Email: valievrashid@mail.ru

Authors

Rinat T. Nasibullin − *Tomsk State University, Tomsk 634050, Russia*

Dage Sundholm − *Department of Chemistry, Faculty of Science, University of Helsinki, Helsinki FIN-00014, Finland;* orcid.org/0000-0002-2367-9277

Theo Kurten − *Department of Chemistry, Faculty of Science, University of Helsinki, Helsinki FIN-00014, Finland;* orcid.org/0000-0002-6416-4931

Hans Ågren − *Department of Physics and Astronomy, Uppsala University, Uppsala SE-751 20, Sweden; College of Chemistry and Chemical Engineering, Henan University, Kaifeng 475004, Henan, P. R. China;* orcid.org/0000-0002-1763-9383

Complete contact information is available at: https://pubs.acs.org/10.1021/acs.jpca.0c09692

Notes

The authors declare no competing financial interest.

ACKNOWLEDGMENTS

This work has been supported by the Olle Engkvist Byggmästare foundation (contract no. 189-0223) and the Ministry of Education and Science of Ukraine (project no. 0117U003908). The calculations were performed with computational resources provided by the High-Performance Computing Center North (HPC2N) in Umeå, Sweden, through the project "Multiphysics Modeling of Molecular Materials" SNIC 2019-2-41. The GIMIC calculations were carried out using the SKIF supercomputer at Tomsk State University. This project has also been funded by the Academy of Finland (projects 315600 and 314821). R.R.V. thanks the Tomsk Polytechnic University Competitiveness Enhancement Program (VIU-RSCABS-142/2019) for support.

REFERENCES

(1) Kaiser, K.; Scriven, L. M.; Schulz, F.; Gawel, P.; Gross, L.; Anderson, H. L. An sp-Hybridized Molecular Carbon Allotrope, Cyclo[18]carbon. *Science* **2019**, *365*, 1299−1301.

(2) Shi, B.; Yuan, L.; Tang, T.; Yuan, Y.; Tang, Y. Study on Electronic Structure and Excitation Characteristics of Cyclo[18]-carbon. *Chem. Phys. Lett.* **2020**, *741*, 136975.

(3) Hussain, S.; Chen, H.; Zhang, Z.; Zheng, H. Vibrational Spectra and Chemical Imaging of Cyclo[18]carbon by Tip Enhanced Raman Spectroscopy. *Chem. Commun.* **2020**, *56*, 2336.

(4) Shi-Xiong, L.; De-Liang, C.; Zheng-Ping, Z.; Zheng-Wen, L.; Shui-Jie, Q. Study on the Ground State Properties and Excitation Properties of C_{18} Under Different External Electric Fields. *Acta Phys. Sin.* **2020**, *69*, 103101.

(5) Baryshnikov, G. V.; Valiev, R. R.; Kuklin, A. V.; Sundholm, D.; Ågren, H. Cyclo[18]carbon: Insight into Electronic Structure, Aromaticity, and Surface Coupling. *J. Phys. Chem. Lett.* **2019**, *10*, 6701−6705.

(6) Fedik, N.; Kulichenko, M.; Steglenko, D.; Boldyrev, A. I. Can Aromaticity Be a Kinetic Trap? Example of Mechanically Interlocked Aromatic [2-5]Catenanes Built from Cyclo[18]carbon. *Chem. Commun.* **2020**, *56*, 2711−2714.

(7) Liu, Z.; Lu, T.; Chen, Q. An sp-Hybridized All-Carboatomic Ring, Cyclo[18]carbon: Bonding character, Electron Delocalization, and Aromaticity. *Carbon* **2020**, *165*, 468−475.

(8) Li, M.; Gao, Z.; Han, Y.; Zhao, Y.; Yuan, K.; Nagase, S.; Ehara, M.; Zhao, X. Potential Molecular Semiconductor Devices: cyclo-C_n (n = 10 and 14) With Higher Stabilities and Aromaticities than Acknowledged cyclo-C_{18}. *Phys. Chem. Chem. Phys.* **2020**, *22*, 4823−4831.
(9) Dai, C.; Chen, D.; Zhu, J. Achieving Adaptive Aromaticity in Cyclo[10]carbon by Screening Cyclo[n]carbon (n=8−24). *Chem.—Asian J.* **2020**, *15*, 2187−2191.
(10) Charistos, N. D.; Muñoz-Castro, A. Induced Magnetic Field in sp-Hybridized Carbon Rings: Analysis of Double Aromaticity and Antiaromaticity in Cyclo[2N]carbon Allotropes. *Phys. Chem. Chem. Phys.* **2020**, *22*, 9240−9249.
(11) Nandi, A.; Solel, E.; Kozuch, S. Carbon Tunneling in the Automerization of Cyclo[18]carbon. *Chem.—Eur. J.* **2020**, *26*, 625−628.
(12) Brémond, É.; Pérez-Jiménez, Á. J.; Adamo, C.; Sancho-García, J. C. sp-Hybridized Carbon Allotrope Molecular Structures: An Ongoing Challenge for Density-Functional Approximations. *J. Chem. Phys.* **2019**, *151*, 211104.
(13) Zou, W.; Tao, Y.; Kraka, E. Systematic Description of Molecular Deformations with Cremer−Pople Puckering and Deformation Coordinates Utilizing Analytic Derivatives: Applied to Cycloheptane, Cyclooctane, and Cyclo[18]carbon. *J. Chem. Phys.* **2020**, *152*, 154107.
(14) Hong, I.; Ahn, J.; Shin, H.; Bae, H.; Lee, H.; Benali, A.; Kwon, Y. Competition between Hückel's Rule and Jahn−Teller Distortion in Small Carbon Rings: A Quantum Monte Carlo Study. *J. Phys. Chem. A* **2020**, *124*, 3636−3640.
(15) Fang, S.; Hu, Y. H. Cyclo[18]carbon as an Ultra-Elastic Molecular O-ring With Unique Mechanical Properties. *Carbon* **2021**, *171*, 96−103.
(16) Zhang, L.; Li, H.; Feng, Y. P.; Shen, L. Diverse Transport Behaviors in Cyclo[18]carbon-Based Molecular Devices. *J. Phys. Chem. Lett.* **2020**, *11*, 2611−2617.
(17) Pereira, Z. S.; da Silva, E. Z. Spontaneous Symmetry Breaking in Cyclo[18]Carbon. *J. Phys. Chem. A* **2020**, *124*, 1152−1157.
(18) Liang, Z.; He, T.; An, J.; Xue, H.; Tang, F.; Fan, D. Coupling Effect and Charge Redistribution of Cyclo[18]carbons and Cyclocarbon Oxides on NaCl Surface. *Int. J. Mod. Phys. B* **2020**, *34*, 2050138.
(19) Jiang, Y.; Mattioli, E. J.; Calvaresi, M.; Wang, Z. Theoretical Design of an Ultrafast Supramolecular Rotor Composed of Carbon Nano-Rings. *Chem. Commun.* **2020**, *56*, 11835−11838.
(20) Liu, Z.; Lu, T.; Chen, Q. An sp-Hybridized all-Carboatomic Ring, Cyclo[18]carbon: Electronic Structure, Electronic Spectrum, and Optical Nonlinearity. *Carbon* **2020**, *165*, 461−467.
(21) Hou, X.; Ren, Y.; Fu, F.; Tian, X. Doping Atom to Tune Electronic Characteristics and Adsorption of Cyclo[18]carbons: A Theoretical Study. *Comput. Theor. Chem.* **2020**, *1187*, 112922.
(22) Scriven, L. M.; Kaiser, K.; Schulz, F.; Sterling, A. J.; Woltering, S. L.; Gawel, P.; Christensen, K. E.; Anderson, H. L.; Gross, L. Synthesis of Cyclo[18]carbon via Debromination of $C_{18}Br_6$. *J. Am. Chem. Soc.* **2020**, *142*, 12921−12924.
(23) Maier, S. An atomic-scale view of cyclocarbon synthesis. *Science* **2019**, *365*, 1245−1246.
(24) Stasyuk, A. J.; Stasyuk, O. A.; Solà, M.; Voityuk, A. A. Cyclo[18]carbon: the smallest all-carbon electron acceptor. *Chem. Commun.* **2020**, *56*, 352−355.
(25) Fowler, P. W.; Mizoguchi, N.; Bean, D. E.; Havenith, R. W. A. Double Aromaticity and Ring Currents in All-Carbon Rings. *Chem.—Eur. J.* **2009**, *15*, 6964−6972.
(26) Wodrich, M. D.; Corminboeuf, C.; Park, S. S.; Schleyer, P. v. R. Double Aromaticity in Monocyclic Carbon, Boron, and Borocarbon Rings Based on Magnetic Criteria. *Chem.—Eur. J.* **2007**, *13*, 4582−4593.
(27) Torelli, T.; Mitas, L. Electron Correlation in C_{4N+2} Carbon Rings: Aromatic versus Dimerized Structures. *Phys. Rev. Lett.* **2000**, *85*, 1702−1705.
(28) Remya, K.; Suresh, C. H. Carbon Rings: a DFT Study on Geometry, Aromaticity, Intermolecular Carbon−Carbon Interactions and Stability. *RSC Adv.* **2016**, *6*, 44261−44271.
(29) Seenithurai, S.; Chai, J.-D. TAO-DFT Investigation of Electronic Properties of Linear and Cyclic Carbon Chains. *Sci. Rep.* **2020**, *10*, 13133.
(30) Valiev, R. R.; Baryshnikov, G. V.; Nasibullin, R. T.; Sundholm, D.; Ågren, H. When are Antiaromatic Molecules Paramagnetic? *J. Phys. Chem. C* **2020**, *124*, 21027−21035.
(31) Zhao, Y.; Truhlar, D. G. The M06 Suite of Density Functionals for Main Group Thermochemistry, Thermochemical Kinetics, Noncovalent Interactions, Excited States, and Transition Elements: Two New Functionals and Systematic Testing of Four M06-class Functionals and 12 other Functionals. *Theor. Chem. Acc.* **2008**, *120*, 215−241.
(32) Weigend, F.; Ahlrichs, R. Balanced Basis Sets of Split Valence, Triple Zeta Valence and Quadruple Zeta Valence Quality for H to Rn: Design and Assessment of Accuracy. *Phys. Chem. Chem. Phys.* **2005**, *7*, 3297−3305.
(33) Becke, A. D. Density-Functional Exchange-Energy Approximation with Correct Asymptotic Behavior. *Phys. Rev. A: At., Mol., Opt. Phys.* **1988**, *38*, 3098−3100.
(34) Lee, C.; Yang, W.; Parr, R. G. Development of the Colle-Salvetti Correlation-Energy Formula into a Functional of the Electron Density. *Phys. Rev. B: Condens. Matter Mater. Phys.* **1988**, *37*, 785−789.
(35) Chai, J.-D.; Head-Gordon, M. Long-Range Corrected Hybrid Density Functionals with Damped Atom−Atom Dispersion Corrections. *Phys. Chem. Chem. Phys.* **2008**, *10*, 6615−6620.
(36) Zhao, Y.; Truhlar, D. G. A New Local Density Functional for Main-Group Thermochemistry, Transition Metal Bonding, Thermochemical Kinetics, and Noncovalent Interactions. *J. Chem. Phys.* **2006**, *125*, 19410.
(37) Roos, B. O.; Lindh, R.; Malmqvist, P. Å.; Veryazov, V.; Widmark, P. O. *Multiconfigurational Quantum Chemistry*; Wiley: Hoboken, NJ, USA, 2016; p 230.
(38) Granovsky, A. A. Communication: An efficient approach to compute statespecific nuclear gradients for a generic state-averaged multi-configuration self consistent field wavefunction. *J. Chem. Phys.* **2015**, *143*, 231101.
(39) Ditchfield, R.; Hehre, W. J.; Pople, J. A. Self-Consistent Molecular Orbital Methods. 9. Extended Gaussian-type basis for molecular-orbital studies of organic molecules. *J. Chem. Phys.* **1971**, *54*, 724−728.
(40) Clark, T.; Chandrasekhar, J.; Spitznagel, G. n. W.; Schleyer, P. v. R. Efficient diffuse function-augmented basis-sets for anion calculations. 3. The 3-21+G basis set for 1st-row elements, Li-F. *J. Comput. Chem.* **1983**, *4*, 294−301.
(41) Frisch, M. J.; Pople, J. A.; Binkley, J. S. Self-Consistent Molecular Orbital Methods. 25. Supplementary Functions for Gaussian Basis Sets. *J. Chem. Phys.* **1984**, *80*, 3265−3269.
(42) Raghavachari, K.; Binkley, J. S.; Seeger, R.; Pople, J. A. Self-Consistent Molecular Orbital Methods. 20. Basis set for correlated wave-functions. *J. Chem. Phys.* **1980**, *72*, 650−654.
(43) Peterson, K. A.; Woon, D. E.; Dunning, T. H., Jr. Benchmark calculations with correlated molecular wave functions. IV. The classical barrier height of the $H+H_2 \rightarrow H_2+H$ reaction. *J. Chem. Phys.* **1994**, *100*, 7410−7415.
(44) Granovsky, A. A. Firefly version 8. http://classic.chem.msu.su/gran/firefly/index.html (accessed 2020-12-09).
(45) Schmidt, M. W.; Baldridge, K. K.; Boatz, J. A.; Elbert, S. T.; Gordon, M. S.; Jensen, J. H.; Koseki, S.; Matsunaga, N.; Nguyen, K. A.; Su, S.; et al. General Atomic and Molecular Electronic Structure System. *J. Comput. Chem.* **1993**, *14*, 1347−1363.
(46) Jusélius, J.; Sundholm, D.; Gauss, J. Calculation of Current Densities Using Gauge-Including Atomic Orbitals. *J. Chem. Phys.* **2004**, *121*, 3952−3963.
(47) Gauge-Including Magnetically Induced Currents (GIMIC) program is distributed on GitHub platform and can be downloaded

through the link. https://github.com/qmcurrents/gimic (accessed 2020-12-09).
(48) Sundholm, D.; Fliegl, H.; Berger, R. J. F. Calculations of magnetically induced current densities: theory and applications. *Wiley Interdiscip. Rev.: Comput. Mol. Sci.* **2016**, *6*, 639−678.
(49) London, F. The Quantic Theory of Inter-Atomic Currents in Aromatic Combinations. *J. Phys. Radium* **1937**, *8*, 397−409.
(50) Frisch, M. J.; Trucks, G. W.; Schlegel, H. B.; Scuseria, G. E.; Robb, M. A.; Cheeseman, J. R.; Scalmani, G.; Barone, V.; Petersson, G. A.; Nakatsuji, H.; et al. *Gaussian 16*, Revision C.01; Gaussian, Inc.: Wallingford CT, 2016.
(51) Arulmozhiraja, S.; Ohno, T. CCSD Calculations on C_{14}, C_{18}, and C_{22} Carbon Clusters. *J. Chem. Phys.* **2008**, *128*, 114301.
(52) Saito, M.; Okamoto, Y. Second-order Jahn-Teller Effect on Carbon 4N+2 member ring clusters. *Phys. Rev. B: Condens. Matter Mater. Phys.* **1999**, *60*, 8939−8942.
(53) Valiev, R. R.; Fliegl, H.; Sundholm, D. Bicycloaromaticity and Baird-Type Bicycloaromaticity of Dithienothiophene-Bridged [34]-Octaphyrins. *Phys. Chem. Chem. Phys.* **2018**, *20*, 17705−17713.
(54) Baryshnikov, G. V.; Valiev, R. R.; Li, Q.; Li, C.; Xie, Y.; Ågren, H. Computational Study of Aromaticity, ^{1}H NMR Spectra and Intermolecular Interactions of Twisted Thia-Norhexaphyrin and its Multiply Annulated Polypyrrolic Derivatives. *Phys. Chem. Chem. Phys.* **2019**, *21*, 25334−25343.
(55) Valiev, R. R.; Benkyi, I.; Konyshev, Y. V.; Fliegl, H.; Sundholm, D. Computational Studies of Aromatic and Photophysical Properties of Expanded Porphyrins. *J. Phys. Chem. A* **2018**, *122*, 4756−4767.
(56) Reiter, K.; Weigend, F.; Wirz, L. N.; Dimitrova, M.; Sundholm, D. Magnetically Induced Current Densities in Toroidal Carbon Nanotubes. *J. Phys. Chem. C* **2019**, *123*, 15354−15365.
(57) Stoychev, G. L.; Auer, A. A.; Izsák, R.; Neese, F. Self-Consistent Field Calculation of Nuclear Magnetic Resonance Chemical Shielding Constants Using Gauge-Including Atomic Orbitals and Approximate Two-Electron Integrals. *J. Chem. Theory Comput.* **2018**, *14*, 619−637.
(58) Salzner, U.; Aydin, A. Improved Prediction of Properties of π-Conjugated Oligomers with Range-Separated Hybrid Density Functionals. *J. Chem. Theory Comput.* **2011**, *7*, 2568−2583.

https://dx.doi.org/10.1021/acs.jpca.0c09692
J. Phys. Chem. A 2020, 124, 10849−10855